Modelling the construction and long-term response of Göta Tunnel

Computers and Geotechnics 134 (2021) 104027

Contents lists available at ScienceDirect

Computers and Geotechnics

journal homepage: www.elsevier.com/locate/compgeo

Research Paper

Modelling the construction and long-term response of Göta Tunnel

Johannes Tornborg [a,b,*], Mats Karlsson [a], Anders Kullingsjö [b], Minna Karstunen [a]

[a] Chalmers University of Technology, Department of Architecture and Civil Engineering, SE-412 96 Gothenburg, Sweden
[b] Skanska Sverige AB, SE-405 18 Gothenburg, Sweden

ARTICLE INFO

Keywords:
Soft clay
Excavation
Rate-dependency
Anisotropy
Earth pressure
Constitutive modelling

ABSTRACT

This paper presents a benchmark of a rate-dependent constitutive model for soft soils, implemented in a 2D finite element code, against the response of an instrumented excavation in sensitive clay: Göta Tunnel in Gothenburg. The monitoring data, which comprise time-series of pore water pressures, displacements, earth pressures and strut forces, provide valuable insights of the time-dependent response during the construction period. The long-term response, in terms of the ongoing settlement rates, is assessed using remote sensing data. The results of the numerical simulations demonstrate that the constitutive model, Creep-SCLAY1S, is capable of capturing the observed response. The trends of vertical and horizontal displacements are captured well until the stage of dewatering, and the evolution of pore pressures and earth pressures is computed with high accuracy, excluding peaks in the measurement values arising from pile and rock anchor installation. Most importantly, the results demonstrate that the rate-dependent model enables to model the complete service life of the tunnel, from construction of the excavation to the tunnel operation, with one unified model parameter set. Furthermore, the comparisons highlight the importance of assessing installation effects both in the choice of construction methods and modelling.

1. Introduction

The increasing demand for infrastructure systems in urban areas, such as railway tunnels, underground water retention systems and deep basements, requires accurate predictions of earth pressures and deformations of retaining structures to facilitate a safe and optimised design. Optimisation is desirable both for economic reasons, as well as essential in minimising the environmental impact of the construction and the permanent structure itself. Predictions of the performance of earth retaining structures for the short-term (construction period) consider both the safety of the workers and the effects on adjacent structures, while the simulations for the long-term performance (design life time of permanent structures) is part of the asset management. Particularly challenging is constructing excavations and structures in soft soils in areas with on-going background settlements (e.g. Zeevaert, 1957; Shen et al., 2014; Wu et al., 2017).

For accurate predictions of the response of geotechnical structures in soft sensitive clays, the numerical model needs to account for characteristic features of natural clay response such as e.g. rate-dependency (including effect of on-going creep settlements) (Crawford, 1964; Bjerrum, 1967; Graham et al., 1983; Lefebvre and LeBoeuf, 1987), anisotropy (Pande and Sharma, 1983; Callisto and Calabresi, 1998; Wheeler et al., 2003; Karlsrud and Hernandez-Martinez, 2013) and destructuration (Leroueil and Vaughan, 1990; Bertoldo and Callisto, 2016). Failure to incorporate the relevant features of the natural soil behaviour in geotechnical design may lead to sub-optimised structures, or even failures such as those described in Magnus et al. (2005), Chen et al. (2015) and Do et al. (2016). Deep excavations in close proximity to existing infrastructure in urban areas also come with strict regulations on the permitted displacements as part of Serviceability Limit State (SLS) considerations. The limitations for the permitted displacements directly affect the mobilised earth pressures acting on the retaining structures both in the short-term, as well as the long-term. Furthermore, as the demand for ever deeper excavations and larger underground spaces is increasing, and accurate predictions are the baseline for the rigorous use of the Observational Method (Peck, 1969), new calculation methods are needed to have confidence in our ability to analyse complex systems.

Previous research related to excavations has been carried out using 2D and 3D finite element analyses in idealised studies (e.g. Potts and Fourie, 1984; Hashash and Whittle, 1996; Zdravkovic et al., 2005; Finno

* Corresponding author at: Chalmers University of Technology, Department of Architecture and Civil Engineering, SE-412 96 Gothenburg, Sweden.
E-mail addresses: johannes.tornborg@chalmers.se (J. Tornborg), mats.karlsson@chalmers.se (M. Karlsson), anders.kullingsjo@skanska.se (A. Kullingsjö), minna.karstunen@chalmers.se (M. Karstunen).

https://doi.org/10.1016/j.compgeo.2021.104027
Received 15 October 2020; Received in revised form 30 December 2020; Accepted 18 January 2021
Available online 6 March 2021

Nomenclature

a	rate of destructuration
b	relative rate of destructuration due to deviator strain rate
c'	apparent cohesion
CSS	current state surface
e_0	initial void ratio
E'	Young's modulus
ICS	intrinsic compression surface
$k_{v,h}$	vertical and horizontal permeability, respectively
K	earth pressure coefficient
K_0	coefficient of earth pressure at rest
K_0^{nc}	coefficient of earth pressure at rest for normally consolidated state
$\overline{K}$	normalised horizontal earth pressure
M_c	stress ratio at critical state in triaxial compression
M_e	stress ratio at critical state in triaxial extension
NCS	normal compression surface
OCR	overconsolidation ratio
p'	mean effective stress
p'_{eq}	equivalent mean effective stress
p'_m	mean effective preconsolidation pressure
q	deviatoric stress
R_{inter}	coefficient for interface friction
S_t	sensitivity
SPW	sheet pile wall
$u_{TPcells}$	pore pressure measured by total pressure cell
V_p	pre-cast concrete pile volume
w_n	natural water content
w_L	liquid limit
α_0	initial anisotropy
α_{xy}	distortional component of fabric tensor
γ	unit weight
γ'	submerged unit weight
$\dot{\varepsilon}^e_{v,q}$	elastic volumetric and deviatoric strain rate, respectively
$\dot{\varepsilon}^c_{v,q}$	viscoplastic volumetric and deviatoric strain rate, respectively
κ^*	modified swelling index
λ_i^*	modified intrinsic compression index
μ_i^*	modified intrinsic creep index
ν'	Poisson's ratio
$\sigma'_{v,h}$	vertical and horizontal effective stress, respectively
σ'_{v0}	initial vertical effective stress
σ'_{vc}	vertical preconsolidation pressure
$\sigma_{h,TPcells}$	horizontal total stress measured by total pressure cell
τ	reference time
ϕ'	friction angle
χ_0	initial amount of bonding
ω	rate of rotational hardening
ω_d	relative rate of rotational hardening due to deviator strain rate

et al., 2007; Karlsrud and Andresen, 2008; Chowdhury et al., 2013; Bertoldo and Callisto, 2019) as well as back-analyses of data from excavations (e.g. Finno and Roboski, 2005; Corral and Whittle, 2010; Orazalin et al., 2015; Whittle et al., 2015; Dong et al., 2016; Rouainia et al., 2017). As the results of numerical analyses depend on the constitutive model chosen, it is important to benchmark the models used not only at element level against laboratory data, but also against full scale field measurements, as pointed out in Whittle et al. (2015). However, studies including field data of the (coupled) short- and long-term performance are not as numerous (e.g. Carder and Darley, 1998; Richards et al., 2007) and in particular not in the setting of soft clay deposits.

In this paper monitoring data from an instrumented excavation as a part of the Göta Tunnel in Gothenburg, Sweden, are revisited in order to benchmark an advanced contemporary constitutive soil model, Creep-SCLAY1S (Wheeler et al., 2003; Karstunen et al., 2005; Sivasithamparam et al., 2015). Creep-SCLAY1S incorporates many characteristic features of soft sensitive clays, and has previously been successfully benchmarked at field scale level for the case of embankment loading (Amavasai et al., 2017; Amavasai et al., 2018). In order to assess the suitability of the model in assisting on excavation design, predictions need to be compared against data from well instrumented excavations in soft clays. In this paper, 2D finite element simulations on the construction of Göta Tunnel as a function of time are compared to the unique measurement data of displacements, pore water pressures, earth pressures and strut forces from the tunnel construction. The data covers over three years of monitoring from the construction stage. The long-term performance is assessed by exploiting remote sensing data from recent InSAR satellite measurements.

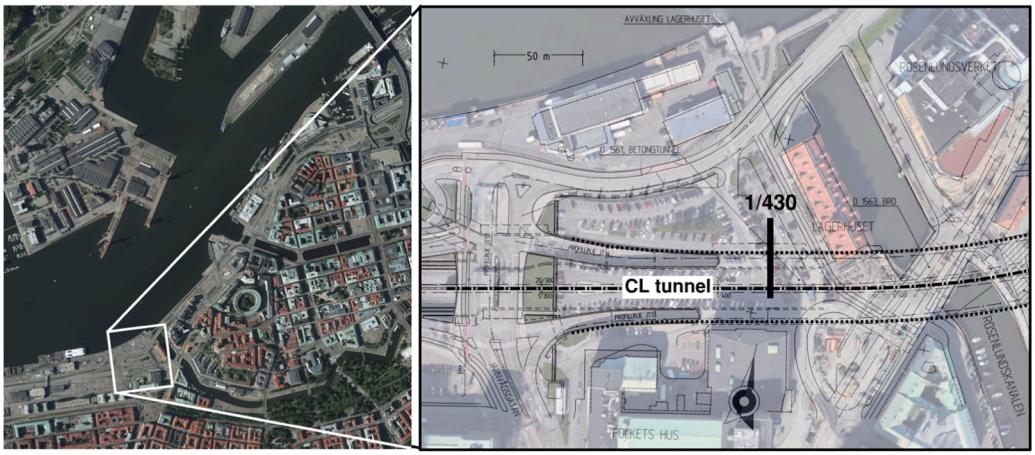

Fig. 1. Overview of the part of Göta Tunnel south of Göta River in Central Gothenburg. The studied section is highlighted, including the centreline and extent of the tunnel.

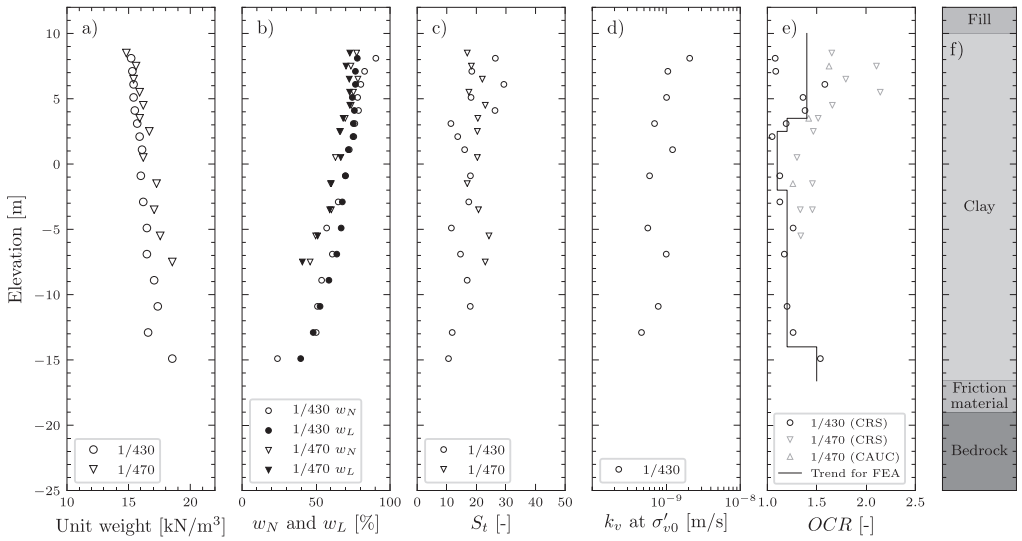

Fig. 2. Index properties of the clay layer(a-c), hydraulic conductivity (d), overconsolidation ratio (e) and soil profile at the location of the sheet pile wall (f).

2. Site description

2.1. Site location and ground conditions

Göta Tunnel is a road tunnel that was constructed in 2000–2006 as a cut-and-cover tunnel. The tunnel, including the Section (1/430) studied, is located in Central Gothenburg, south of Göta River, see Fig. 1. The section studied is located just north of Järntorget and a five-story building from the 1950s. A four-story building from the 1920s is located north-east of the studied section. Both of these buildings have pile foundations, and during the excavation a special concrete support structure was constructed for the 1920s building. Thus, these foundations have not been modelled in the simulations.

The geology in the Göta River valley is dominated by deep deposits of soft sensitive clays formed during and after the last ice-age (glacial and post-glacial clays), reaching depths of over 100 m in Central Gothenburg. The deposits of soft natural clay, in combination with considerable amount of fills, carried out mainly in the 19th century to expand the city, have contributed to significant on-going creep settlements within the city.

The ground surface at the site corresponded to level +12 (Swedish reference system RH2000) before excavation. The top layer consists of 2 m of fill to approximately level +10. A layer of soft sensitive homogeneous clay is found down to approximately level −16 at the location of the studied sheet pile wall, corresponding to 28 m depth below ground surface. With the exception of the fills and a possible weathered crust, the clay layers can be assumed to be fully saturated. Below the clay layer, there are some meters of coarse grained material on top of the bedrock (granodiorite).

The index properties of the clay in the studied section and an adjacent Section (1/470) are presented in Fig. 2. Cone penetration tests (CPT), field vane and fall cone tests indicate an undrained shear strength (uncorrected with respect to liquid limit) of 15 kPa at level +10, with an increase of approximately 1 kPa/m with depth. The vertical hydraulic conductivity (permeability), k_v, has been evaluated from Constant Rate of Strain (CRS) oedometer tests at effective stress levels corresponding to the initial vertical effective stresses in situ. According to Fig. 2 d) k_v ranges from 0.5–2 $\times 10^{-9}$ m/s. The horizontal and vertical permeability of the clay at the site are assumed to be equal based on previous tests on Bäckebol clay (Larsson, 1981), approximately 10 km upstream in Göta River valley. The unit weight of the clay ranges from 15 kN/m^3 in the top of the clay layer to around 18 kN/m^3 at the bottom. The sensitivity varies between 10–25, and is consistent with the measured in situ water content, w_n, that is very similar to the liquid limit, w_L.

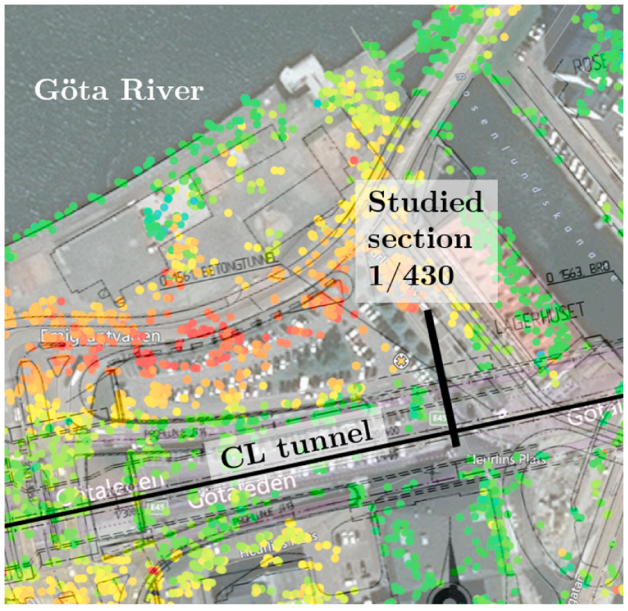

Fig. 3. InSAR satellite data of settlement rates in the area in 2019. Green = 0 mm/year to red ⩾10 mm/year (image courtesy of the Swedish Transport Administration).

The overconsolidation ratio (OCR) varies from 1.1–1.4 in the studied section, based on the apparent preconsolidation pressures evaluated from CRS tests and undrained K_0-consolidated triaxial compression tests. In the adjacent section, 1/470, OCR varies from 1.4–2.0. The high variability in OCR results from the anthropogenic loading history: warehouses for storage of iron were located in the subarea of Section 1/470. The rate of settlement before construction works commenced varied between 3–8 mm/year on the site based on surveying of asphalt surfaces in the area around the section of interest (Svahn and Liedberg, 2001). Based on remote sensing data provided by the Swedish Transport Administration, the current settlement rate just north of the tunnel is ca 2–6 mm/year, Fig. 3. Such variation in settlement rates is typical within the city of Gothenburg, mainly attributed to the anthropogenic loading history (e.g. old canals, harbour basins and piers). Fig. 3 highlights the challenges in the design and construction in areas with on-going settlements as the new structures should be designed to settle at the same

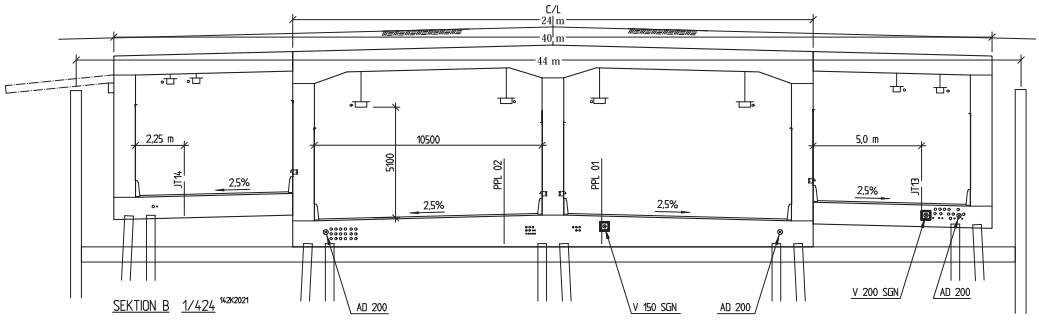

Fig. 4. Cross section of the tunnel structure including ramp segments.

Fig. 5. The excavation after final dewatering in August 2003.

rate as the surrounding soil.

2.2. The permanent structure

A cross section of the permanent tunnel structure is presented in Fig. 4. Göta Tunnel comprises a main structure with a width of 24 m. In the section studied the main tunnel is complemented by additional ramp segments that extend the total width of the structure to 40 m. The foundation contains rows of 0.4 × 0.4 m^2 pre-cast concrete piles, which were driven into the coarse grained soil layer, alternatively to the bedrock. The piles were installed with an out-of-plane centre to centre (c.t.c) distance varying between 2.0–2.5 m.

2.3. Earth retaining structure and construction sequence

The design of the earth retaining system was based on independent analyses by the contractor (Skanska). The excavation was carried out within embedded sheet pile walls (SPWs) with an AZ36 profile (steel grade S355 and L = 26 m). After the installation of the SPWs, a pre-excavation was carried out to level +10 (2 m depth), followed by the installation of the pre-cast concrete piles. In order to minimise mass-displacement and the potential damage to the surroundings, soil was extracted down to level ±0 before installation of each pile. This was carried out by driving a hollow cylinder with an area corresponding to that of the concrete piles and equipped with a trapper in the end. The pile heads were then driven to level +3 in general. This resulted in mass displacements below level ±0 and a net outtake of volume above level +3.

The actual excavation, including casting of a 0.7 m thick concrete sealing slab, was carried out under water. Steel struts (∅711–14.2 mm) were installed at level +13 with a c.t.c distance of 9 m, sequentially with the progress of excavation. Before dewatering, the slab was secured against uplift by the installation of vertical pre-stressed anchors (∅36

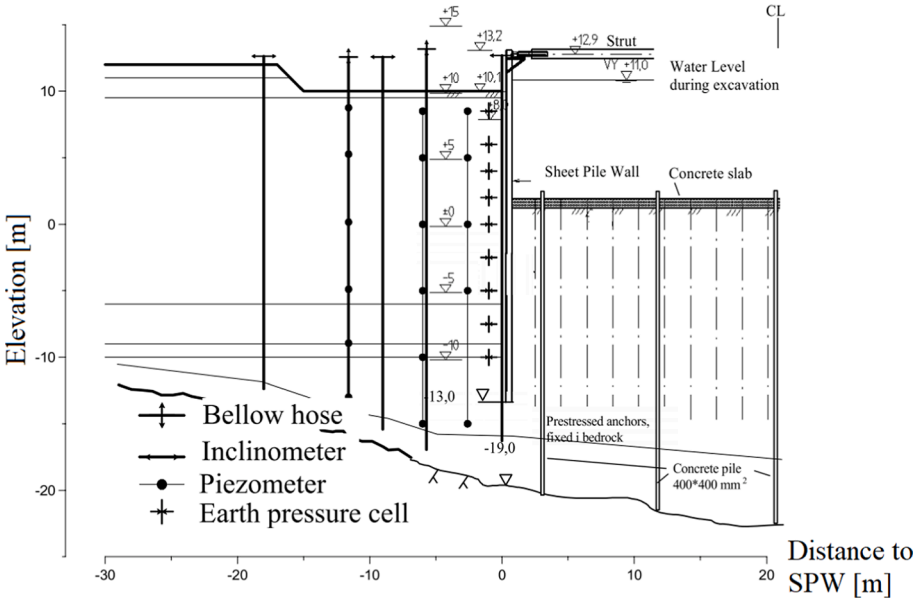

Fig. 6. Instrumentation in Section 1/430 (Kullingsjö, 2007).

mm steel rods) grouted 6 m into the bedrock using an early form of ODEX-drill system (Fang, 1991). Final dewatering took place in August 2003, see Fig. 5. After dewatering, the piles were cut to final levels and construction of the tunnel started.

2.4. Instrumentation

In addition to the process monitoring by the contractor, the excavation was monitored with additional instruments as part of a prior research project (Kullingsjö, 2007). The instrumentation in Section 1/430 is outlined in Fig. 6. In addition to the instrumentation shown, strut forces were also monitored, as well as surveying the displacements of the anchored concrete slab, the buildings nearby and the SPWs themselves.

3. Numerical model of Göta tunnel

3.1. Constitutive model

In order to simulate the time-dependent response during the construction process, as well as the long-term performance, a model that accounts for rate-dependency is required. This also enables to model the on-going background creep settlements. Additionally, the sensitive clay exhibits highly anisotropic response and pronounced strain softening. Significant rotation of principal stress axes is expected when modelling deep excavation problems, and this has a major effect on the clay response (Pande and Sharma, 1983). The numerical analyses were carried out with the Creep-SCLAY1S model, for details about the model formulation see (Wheeler et al., 2003; Karstunen et al., 2005; Sivasithamparam et al., 2015) and Appendix A. The model incorporates the following characteristic soft clay features:

- Rate-dependency; accounts for viscous effects, typical for natural clays (Lefebvre and LeBoeuf, 1987) and mapping the strain rates in the laboratory with the strain rates in the field, consistently accounting for the strain-rate dependence of the mobilised stiffness and shear strength.
- Anisotropy; accounts for the initial anisotropy of Gothenburg clay, as well as the evolution of anisotropy, by incorporating an inclined Normal Compression Surface (NCS) and a rotational hardening law. The latter is computationally more effective than adopting multilaminate framework (Pande and Sharma, 1983) and thoroughly validated experimentally (Karstunen and Koskinen, 2008).
- Destructuration; accounts for the possible loss of strength and stiffness (Finno and Nerby, 1989) due to degradation of bonds in soft sensitive clays (Karlsrud and Andresen, 2008), as well as modelling installation effects (Karlsson et al., 2019; Castro et al., 2014). Both anisotropy and destructuration are assumed to evolve as a function of viscoplastic (creep) volumetric, $\dot{\varepsilon}_v^c$, and deviatoric, $\dot{\varepsilon}_q^c$, strain rates.

One of the main benefits of using a rate-dependent effective stress model is that the same set of parameters can be used both in the short- and the long-term simulations. By using a model that is able to represent the key features of the natural clay tested, the calibration of parameters is actually simpler than with an overly simple model (Gras et al., 2017). Thus, despite the large number of model parameters, a unique set of parameters can be derived for Creep-SCLAY1S following the procedures in Gras et al. (2017) and Gras et al. (2018), provided the necessary standard testing is available. Simplifications of natural clay behaviour that may lead to unsafe design (Karlsrud and Andresen, 2008) are thus avoided. Separating the roles of consolidation and creep in the modelling would require additional analyses switching to a model formulation without creep, which was not the scope of the paper. The Creep-SCLAY1S model does not yet account for the small-strain stiffness, which may be important to consider in modelling the far field response (Jardine et al., 1986; Scharinger et al., 2009).

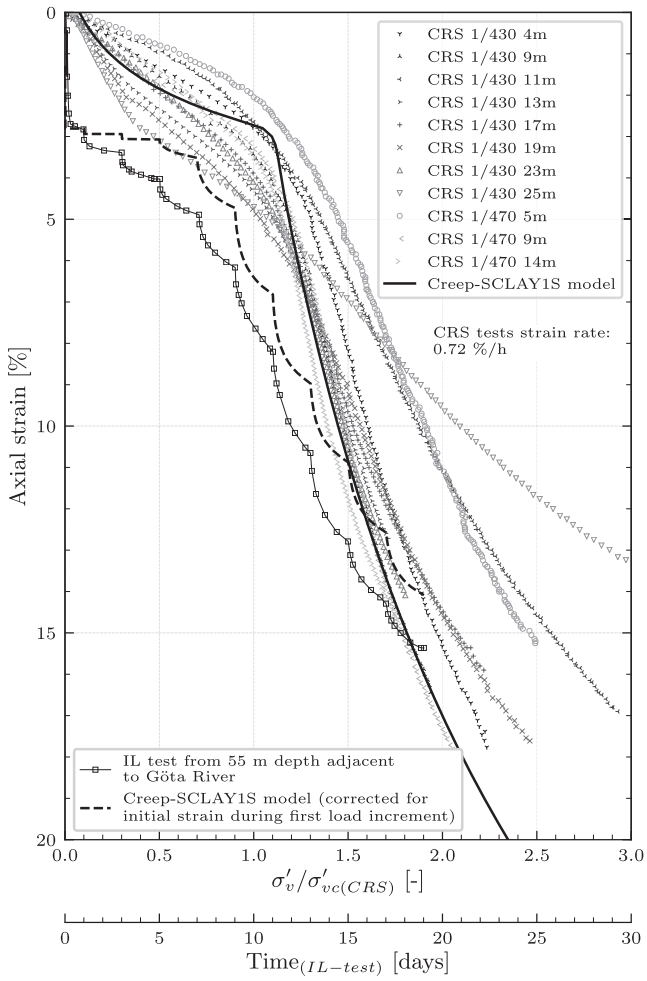

Fig. 7. Model calibration versus CRS test results, as well as calibration against incremental loading (IL) test on a sample from 55 m depth close to Göta River. Note: IL test plotted as strain versus time.

3.2. Model parameters

The design of deep excavations is often based on rudimentary site characterisation (Karlsrud and Andresen, 2008). However, for the case of Göta Tunnel, systematic series of laboratory tests were available, involving oedometer and triaxial tests (Kullingsjö, 2007). Examples of the laboratory data available are presented in Figs. 7 and 8. The CRS tests in Fig. 7 have been normalised with the apparent preconsolidation pressure evaluated from the respective test. The value of K_0^{nc} (coefficient of earth pressure at rest for normally consolidated state) was set to 0.42 in the Creep-SCLAY1S model, matching the value based on Jaky's formula with a friction angle derived from the stress ratio at critical state in triaxial compression, M_c. It should be noted that the value for K_0^{nc} is consequently lower than previously measured in laboratory tests on Gothenburg clay (ranging from 0.50–0.55) (Kullingsjö, 2007; Sällfors, 1975; Olsson, 2013).

Since the initial analyses of the Göta Tunnel excavation with the Creep-SCLAY1S model in Tornborg et al. (2019), new incremental loading (IL) oedometer tests were made available by Larsson (2018). These IL tests were performed on samples from depths greater than 55 m from a nearby site, and the results were used for estimating the values for the modified intrinsic creep index μ_i^*, as this is not possible based on CRS tests alone. Thus, minor adjustments of the model parameters (λ_i^*, ω and μ_i^*) were made compared to Tornborg et al. (2019). Element level simulation of an IL test is included in Fig. 7 plotted as vertical strain

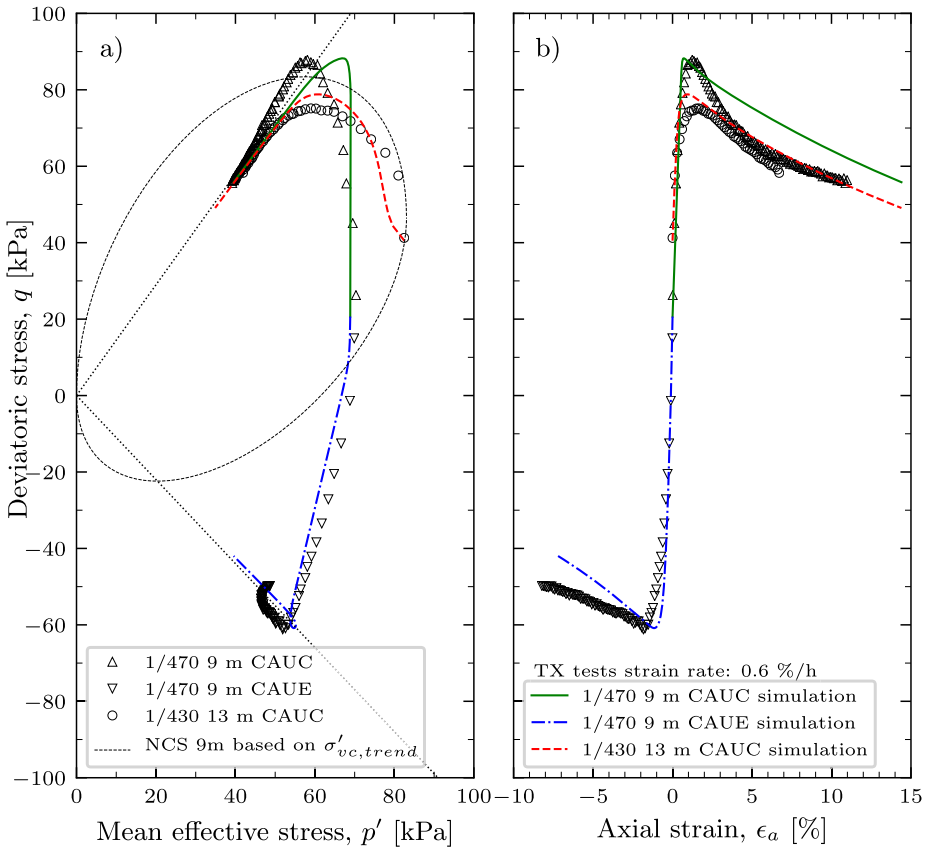

Fig. 8. Examples of K_0-consolidated undrained triaxial tests sheared in compression (CAUC) and extension (CAUE) from Sections 1/430 and 1/470 vs. simulations; (a) p'-q-space; (b) plot of ε_a-q. Test 1/430 was consolidated to $\sigma'_{vc(CRS)}/\sigma'_v$=0.94 before shearing whilst in the simulation the OCR was set to 1.

Table 1
Creep-SCLAY1S model parameters for natural Gothenburg clay at Göta Tunnel.

Parameter	Definition	Value
λ_i^*	Modified intrinsic compression index	0.085
κ^*	Modified swelling index	0.013
ν'	Poisson's ratio	0.20
M_c	Stress ratio at critical state in triaxial compression	1.45
M_e	Stress ratio at critical state in triaxial extension	1.10
ω	Rate of rotational hardening	200
ω_d	Relative rate of rotat. hardening due to deviator strain	1.0
a	Rate of destructuration	8
b	Relative rate of destructuration due to deviator strain	0.5
α_0	Initial anisotropy	0.57
χ_0	Initial amount of bonding	15
μ_i^*	Modified intrinsic creep index	0.0018
τ	Reference time (days)	1

versus time. The simulation of the IL test on the sample from 55 m depth overestimates the stiffness in the elastic region due to the value of κ^* being derived from samples from 4–25 m depth at Göta Tunnel. The element level simulation of a CRS test is also shown, demonstrating that the destructuration law in the model formulation is able to capture the clay response.

The simulations of the K_0-consolidated undrained triaxial compression and extension tests are presented in Fig. 8. Whilst normally the shearing is started after consolidation to the estimated in situ effective stress level (open triangles), for one of the tests the consolidation was taken to $\sigma'_{vc(CRS)}/\sigma'_v$=0.94 (open circles) before shearing. The latter was simulated assuming the soil to be normally consolidated. The undrained

Table 2
Additional model parameters for the clay layers at Göta Tunnel.

Layer	Elevation	γ [kN/m^3]	OCR [–]	e_0 [–]	k_h=k_v [m/s]
1	+10 to +3.5	15.3	1.40	2.26	1×10^{-9}
2	+3.5 to +2.5	15.7	1.20	2.10	1×10^{-9}
3	+2.5 to −2.0	15.9	1.10	1.99	1×10^{-9}
4	−2 to −14	16.8	1.20	1.55	7×10^{-9}
5	below −14	17.9	1.50	0.96	7×10^{-10}

triaxial extension tests allow for calibrating model parameter ω, controlling the rate of evolution of anisotropy. Overall, with the chosen set of parameters, Creep-SCLAY1S is able to represent well both the pore pressure development during shear (i.e. the stress path) and the stress–strain response under undrained deviatoric loading, both in compression and extension. Typical for sensitive clays is the notable strain-softening at rather small strains, which is partly constitutive, i.e. associated with sudden collapse of the apparent bonding, and partly due to localization. The values for the Creep-SCLAY1S model parameters for the clay layers used in the modelling are presented in Tables 1 and 2, and for the fill and coarse grained material in Table 3. The following notations apply to Tables 2 and 3: e_0 initial void ratio, k_v and k_h hydraulic conductivity (permeability) in vertical and horizontal directions, respectively, γ unit weight, γ' submerged unit weight, E' Young's modulus, ν' Poisson's ratio, c' apparent cohesion, ϕ' friction angle and K_0 coefficient of earth pressure at rest.

3.3. Numerical model

The excavation was modelled using a 2D finite element code (Plaxis 2D version 2019). The geometry of the numerical model is given in Fig. 9

Table 3
Parameters for the fill and the coarse grained material below the clay layer.

Material set	γ/γ' [kN/m^3]	E' [MPa]	ν' [–]	c' [kPa]	ϕ' [°]	K_0 [–]
Mohr–Coulomb	18/10	30	0.2	1	35	0.43

and consists of 7252 triangular 6-noded elements. The properties of the structural elements are summarised in Table B1 in Appendix B. The construction sequence was modelled as a time-dependent process of the various construction activities and the intermediate stall-times, based on the actual project logbooks, see Table B2 in Appendix B.

The effect of nearby buildings have not been included in this study, as they are on pile foundations. Due to the sloping bedrock surface, gravity loading was used to generate the initial stresses. The gravity loading was carried out with an elastic model, using a Poisson's ratio of 0.38 to match the desired in situ value of K_0=0.6. This general value was inferred from the equation by Schmidt (1966) which for the OCR values in the studied section, results in the in situ K_0 varying between 0.56–0.64. The subsequent stage involved switching to the Creep-SCLAY1S model, and a plastic nil step was added to initialise the state variables of the constitutive model for the subsequent analyses (see Table B2 for calculation phases).

The following assumptions were made with respect to the boundary conditions and structural elements:

- The excavation was modelled as a 2D plane strain problem. Only the north side of the excavation, containing the instrumentation, was studied and a symmetry line was introduced at the centre-line of the tunnel structure. As discussed, existing buildings were not included in the model.
- The steady state pore pressures were based on piezometer readings, indicating a ground water level at +10 (the top of the clay layer), with an hydrostatic increase with depth.
- The sheet pile wall and the vertical model boundaries were assumed to be impermeable, except for the lower parts of the vertical boundaries, where coarse grained material was present. The model boundary below the coarse grained material (i.e. the bedrock interface) was modelled as impermeable. At the bedrock the displacements were fixed both in the vertical and horizontal directions.
- For the interface between the clay and the wall full friction was assumed (due to the long time of construction before final excavation) with a friction angle of ϕ'=35° and c'=0.1 kPa.
- The concrete slab poured under water was modelled as a solid with material properties in Table B1.

3.4. Modelling installation effects

While we assumed the SPW to be wished-in place, previous analyses in Kullingsjö (2007) indicated that some of the other installation effects had to be accounted for, even if in a simplified manner. Thus, the installation effects due to the pile driving of the pre-cast concrete piles, including outtake of volume with the hollow cylinder, were modelled with a prescribed negative volumetric strain above level +3, no volumetric strain between level +3 and ±0, and positive volumetric strain below level ±0. The ten pile rows in the section were installed in pairs (Fig. 4). The total volumetric strains for each pair of pile rows were calculated and "smeared" over 2 m wide soil clusters in phases 07–09 (Table B2) according to:

$$\varepsilon_v = \frac{2\text{m} \times \text{pile}_{\text{c.t.c;out-of-plane}} + V_p}{2\text{m} \times \text{pile}_{\text{c.t.c;out-of-plane}}} = 1 + V_p / \left(2\text{m} \times \text{pile}_{\text{c.t.c;out-of-plane}}\right) \quad (1)$$

where V_p is pile volume. This corresponds to a volume increase of 8 % for each meter depth in the 2 m wide soil cluster containing the pile row pair in the centre-line and 6.5 % for the other pile row pairs. The total volumetric strains were assumed to be distributed between the horizontal and out-of-plane directions. The (negative) volumetric strain above level +3 was set to −4 % and −2 % for the centre-line and the other pile rows, respectively. As a consequence of the volume change, there will be degradation of bonding in the model, resulting in a disturbed zone around the piles. There are, however, more elegant ways to model pile installation, see e.g. Karlsson et al. (2019).

The concrete piles were modelled as embedded beams. During the pre-stressing of the vertical anchors, and the building of the tunnel and the ramps onto the concrete slab (Table B2 phases 17, 23 and 25), the concrete piles were connected to the lower model boundary. In the other calculation phases, the pile toes were assumed to be free to move, in order not to overestimate the resistance to the uplift forces. The main analysis, discussed in this paper, did not include modelling the installation effects resulting from drilling the vertical anchors. Subsequently, a sensitivity study was made for which the effects of installation of anchors was done, but this did not substantially influence the results.

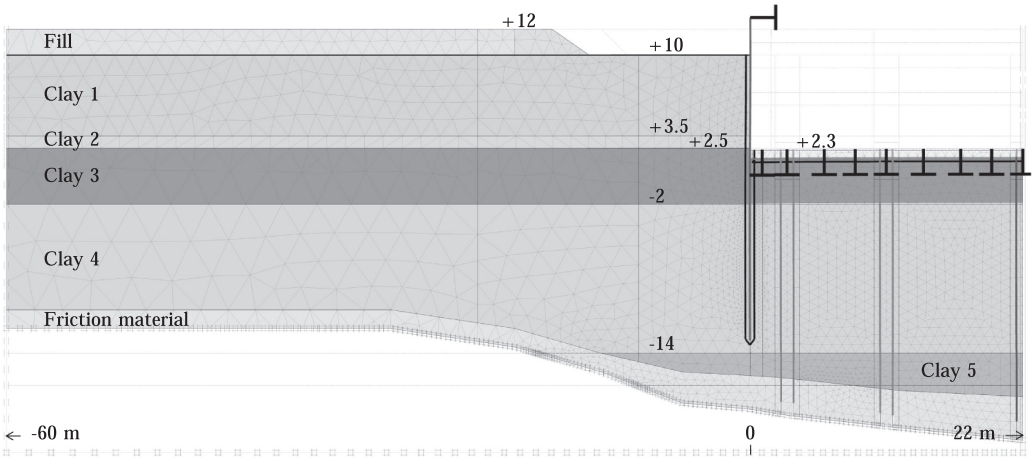

Fig. 9. Numerical model geometry including the finite element mesh for Göta Tunnel excavation (here represented at the stage after dewatering).

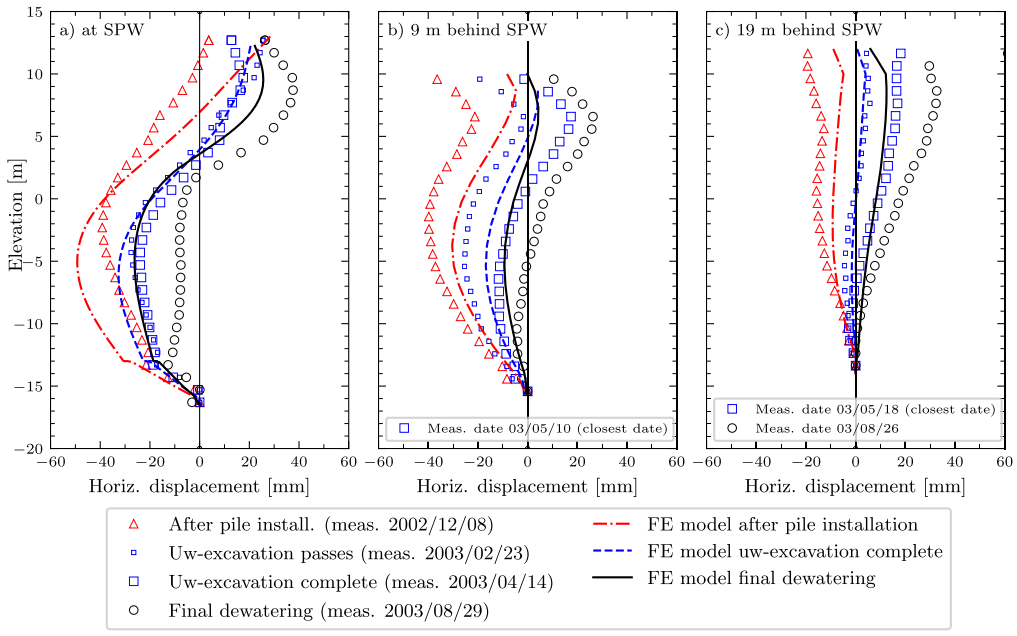

Fig. 10. Measured versus computed horizontal displacements at various distances from SPW. Positive values indicate displacement towards the excavation.

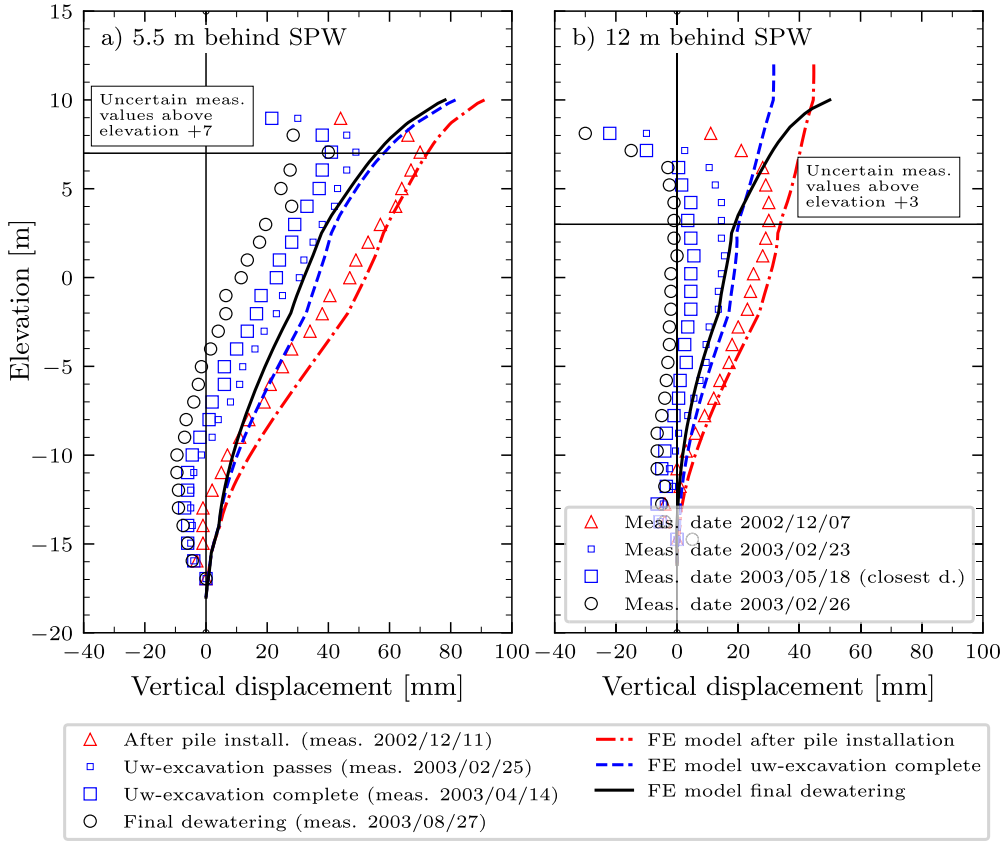

Fig. 11. Measured versus computed vertical displacements at various distances behind SPW. Positive values indicate heave.

4. Results and discussion

This section is divided into three subsections that compare the computed results with field measurements: the response during three main construction stages, the response over a time-series of ca. 2 years after the final dewatering of the excavation, and the background settlement rates. Finally, we discuss the role of evolving anisotropy and destructuration when modelling this problem.

4.1. Response during main construction stages

The comparisons of model simulations with the measurement data consider three main stages of the construction process; i.e. after the pile installation, the underwater excavation and the final dewatering. The

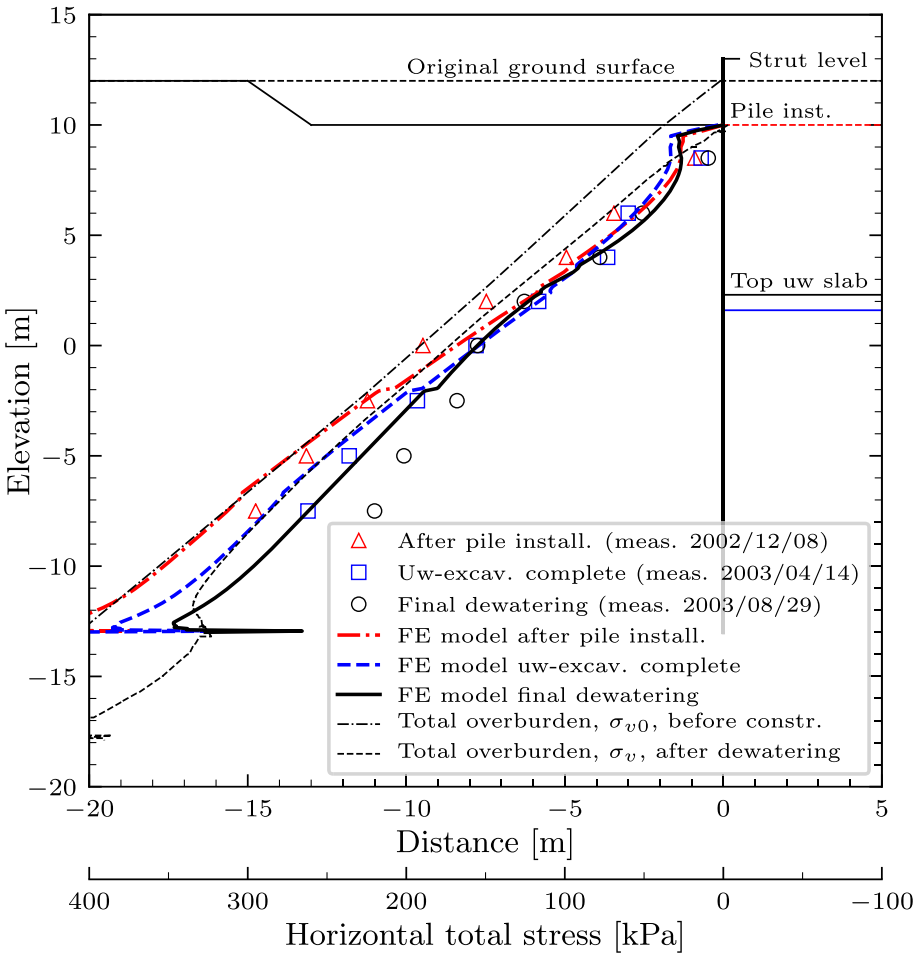

Fig. 12. Measured and computed horizontal total stresses 0.5 m behind SPW. For comparison the total vertical overburden (from the model) at two stages is also included.

horizontal and vertical displacements are plotted in Figs. 10 and 11, respectively, and the horizontal total stresses in Fig. 12. In general, the simulations capture the trends of the displacements well, although the absolute values are off by a maximum of 30 mm in the horizontal and 24 mm in the vertical direction.

For the stage after the pile installation (red markers and lines in Figs. 10 and 11), any differences between the measurements and computed results are considered to be an effect of the simplified modelling of the pile installation process by prescribing volumetric strains. The pre-extraction of soil down to level ±0 was modelled as a negative volumetric strain (collapse). This clearly is an over-simplification, as the results indicate that the "smearing" in the 2D-model underestimate the stiffness response of the clay that in the field can partially arch around the cavities.

After the underwater excavation and final dewatering, the model underestimates the horizontal displacements towards the excavation. This is, to some extent, due to the wished-in-place modelling of the pre-stressed vertical anchors securing the slab against uplift. In reality, the anchors were pre-stressed sequentially under water without post-tensioning, thus most likely not operating under the prescribed pre-stress force at the time before dewatering. Most importantly, the installation of the anchors may have disturbed the clay and the coarse grained material. Part of the underestimation can also be related to the temperature effects and shrinkage of the concrete slab, as discussed by Whittle et al. (1993).

The vertical displacements at 5.5 m and 12 m behind the SPW are shown in Fig. 11. The heave is computed well after the pile installation, but is overpredicted after the final dewatering. The inclusion of small strain stiffness could improve the computed results.

Fig. 12 shows that the computed horizontal total stresses at 0.5 m behind SPW (on the retained side) agree well with the measurements. Included in Fig. 12 is also the total overburden pressure before the start of construction, and at the stage of final dewatering, obtained from the numerical model (dashed black lines). At and below level ±0 the measured total horizontal stresses approach the total initial vertical overburden. This is most likely partly caused by an increase in the horizontal stresses due to the pile-installation.

Comparing our results to previous modelling (Kullingsjö, 2007) that used an anisotropic model for the undrained situation, without considering consolidation and creep, the computed results are similar w.r.t. deformations during the construction stage. The main benefit of using the Creep-SCLAY1S model is, however, the ability to simulate the response with the same set of parameters both in short- and long-term. The rate-dependency also enables accounting for the background creep deformations.

4.2. Response over time

This section compares the computed results with the monitoring data extending for ca. 2 years after final dewatering. Fig. 13 presents the measured and computed pore pressures at different depths and locations behind the SPW. Included on top for clarity is the construction sequence with excavation and water levels. The arrows point to the phases that were discussed in the previous section (Figs. 10–12). The measurements indicate that installation of the sheet pile walls caused notable excess pore pressures close to the wall (the SPWs were installed mid July 2002),

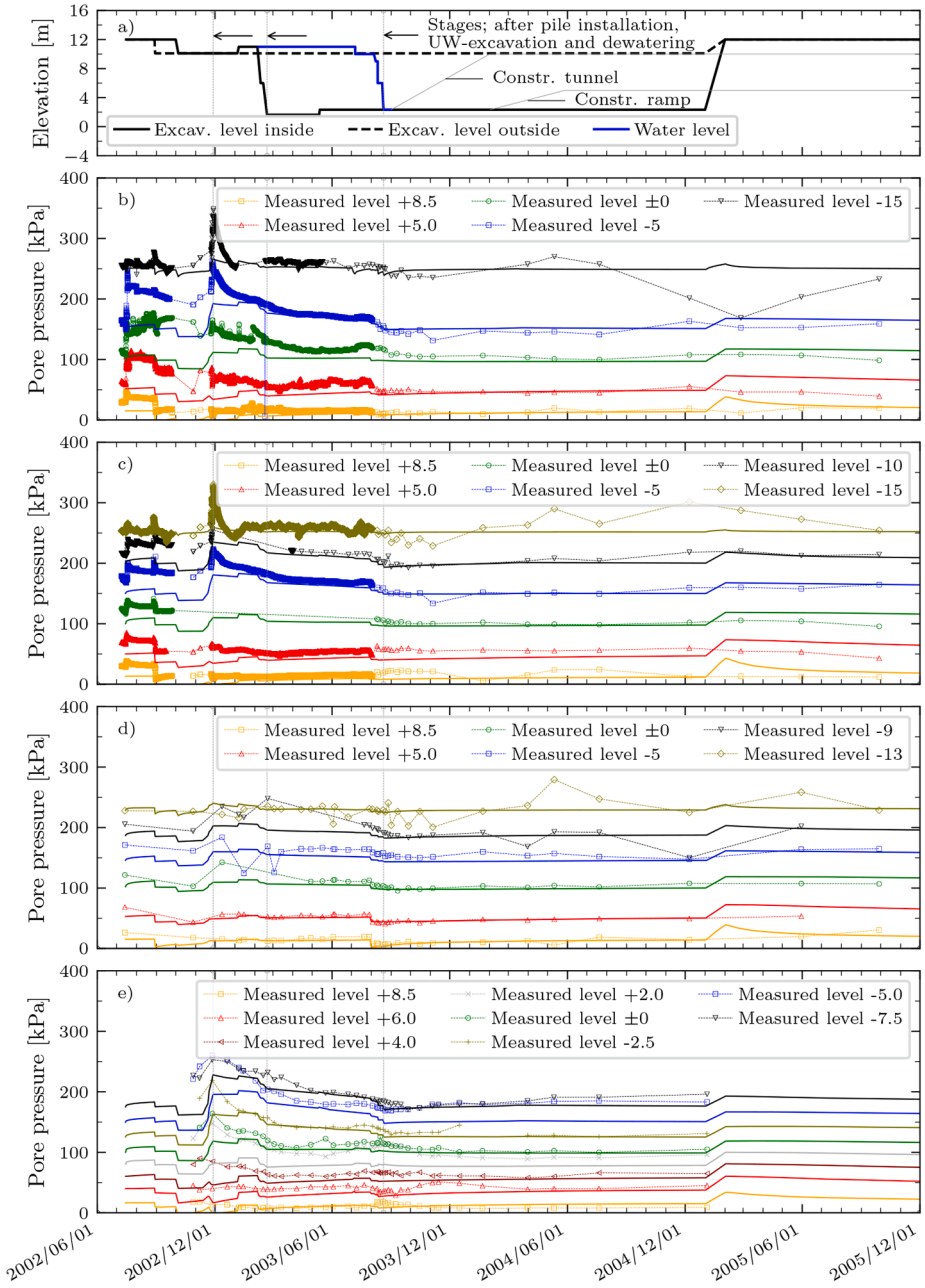

Fig. 13. Measured and computed pore pressures a) construction sequence b), c) and d) piezometers located 2.0, 5.5 respectively 10.0 m behind the SPW and e) piezometers in earth pressure cells 0.5 m behind SPW. Solid lines with no symbols indicate computed results.

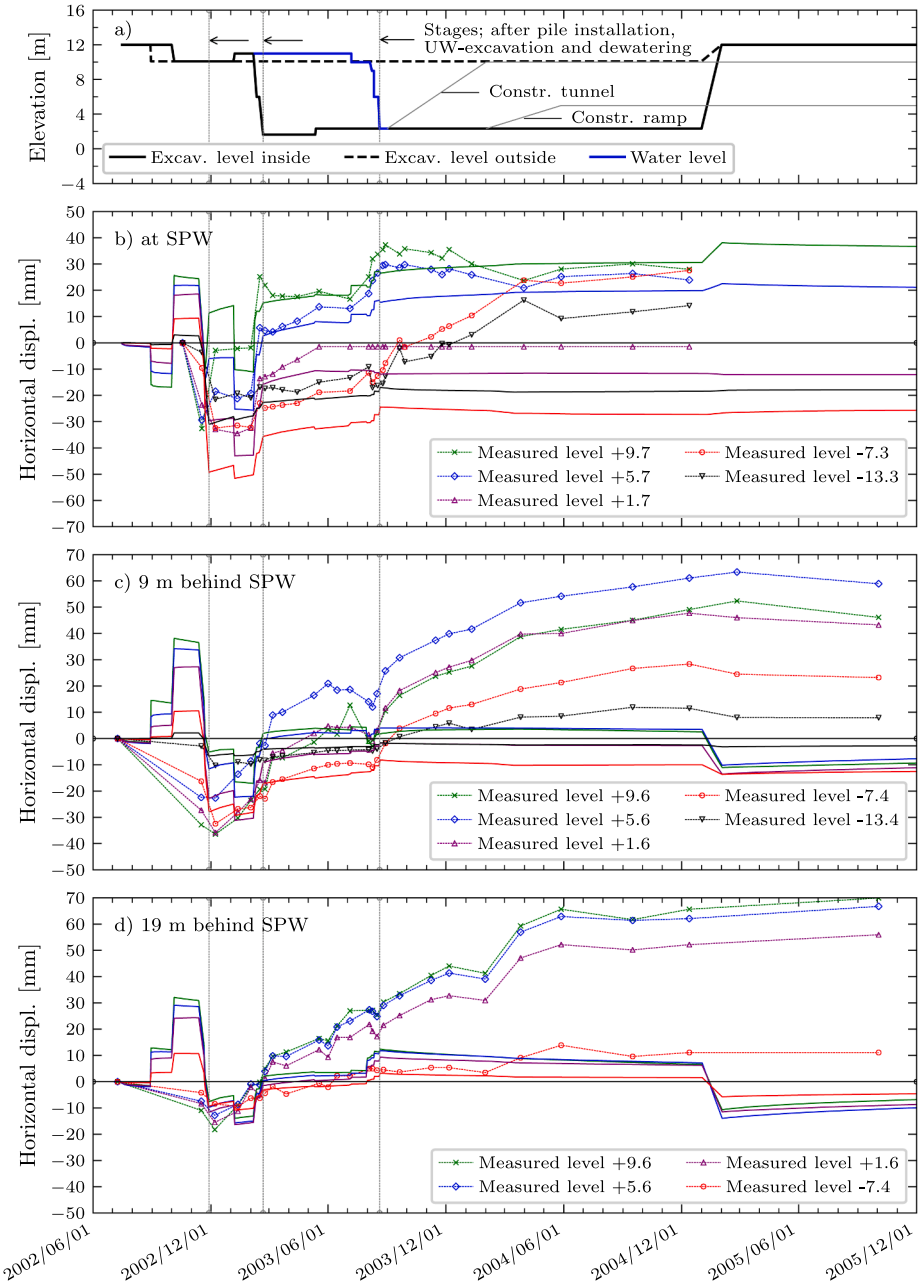

Fig. 14. Measured and computed horizontal displacements a) construction sequence b), c) and d) inclinometers at SPW, 9 and 19 m behind SPW, respectively. Solid lines with no symbols indicate computed results. Positive values indicate displacement towards excavation.

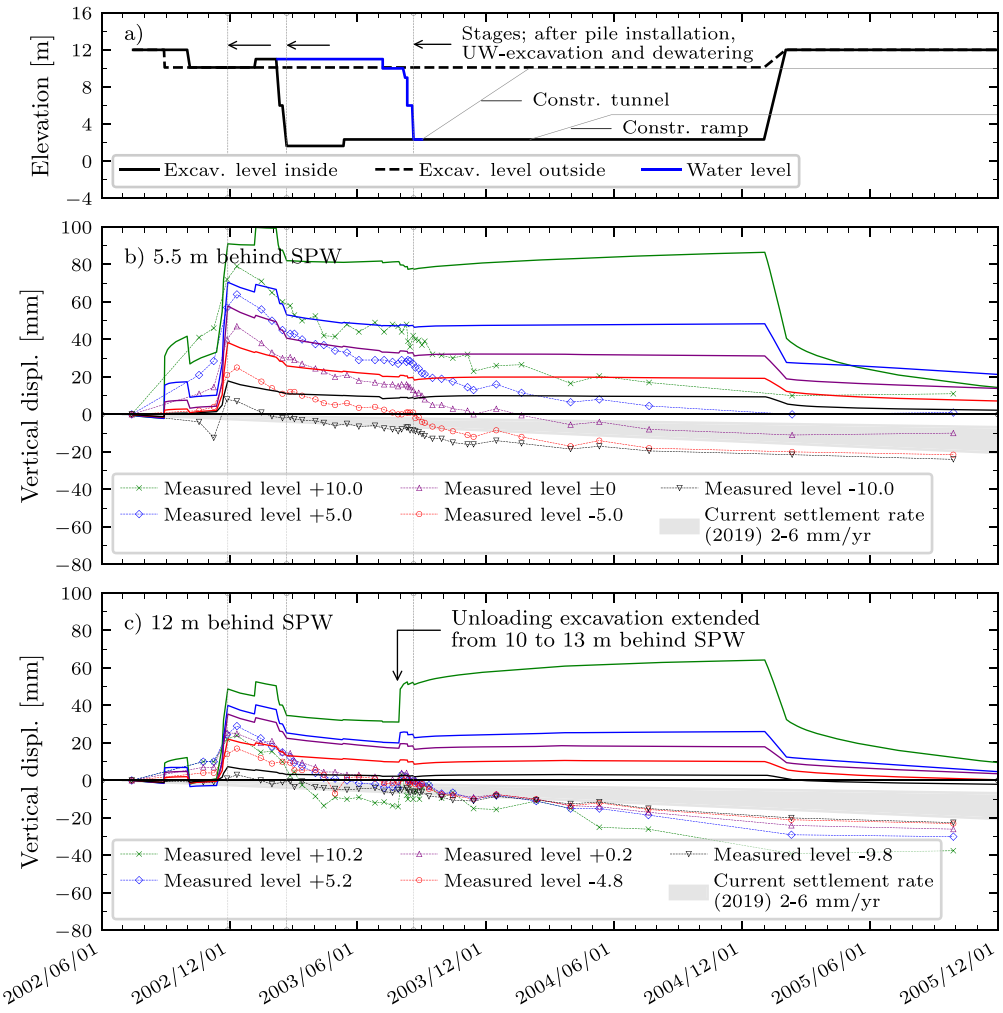

Fig. 15. Measured and computed vertical displacements a) construction sequence b) and c) extensometers at 5.5 and 12 m behind SPW, respectively. Solid lines with no symbols indicate computed results. Positive values indicate heave.

which however dissipated very quickly. The model response seems to be sensitive to the initial pre-excavation. The extreme peaks in pore pressures during pile installation are not captured by the model, due to the simplified modelling of the pile installation process that ignored shearing. Nevertheless, the computed results are in excellent agreement with the measurements at the time of final dewatering and thereafter.

The horizontal and vertical displacements are plotted versus time in Figs. 14 and 15. Again, the construction sequence is included in the top of the Figures. In the measurements, the horizontal displacements (Fig. 14) continued to develop towards the excavation up to ca 9 months after the final dewatering, which is not captured by the model. Whilst the computed results close to the surface (level +9.7) next to the wall are reasonably good, the discrepancies increase further down and further away from the wall. The results indicate that these time-dependent deep horizontal movements were significant, far exceeding the horizontal movements during the construction. In line with these horizontal movements, the extensometers behind the SPW (Fig. 15) also showed additional settlements, while the computed results indicate significant heave. So, there is a mechanism that the model does not fully capture.

Due to these discrepancies, detailed examinations were made to find plausible explanations, considering several possibilities e.g. the vertical upward movement of the anchored concrete slab, the lowering of the pore pressures around the excavation and the shift/horizontal deformation of the entire earth retaining system. Furthermore, the project log-books and photos were revisited. Based on this detailed examination, the continued deformations were most likely caused in part by a shift of the entire earth retaining system to the south (10–20 mm horizontal displacement), but also, to a great extent, by the installation of the vertical anchors within the studied section, as well as an adjacent part of the tunnel excavation. The severe impact of installation effects from ODEX drilling is also observed in field trials (Lande and Karlsrud, 2015) at a well characterised soft clay site (Onsøy, Norway), in comparable ground conditions to those at Göta Tunnel. Additional examples of installation effects due to drilling are given, for example, in Kempfert et al. (1999).

The time-series of the total horizontal stresses and strut forces, as well as the registered ambient air temperature (Swedish Meteorological and Hydrological Institute, 2020) are presented in Fig. 16. Again, the construction sequence is plotted in the top of the Figure. In general, the computed results of total stresses are in good agreement with the monitoring data, although the differences increase with depth. Similarly to the pore pressures, the extreme peak values registered during pile installation are not captured by the model. The computed strut force is in good agreement with the monitoring data. Yet, as the successive installation of struts during underwater excavation was not simulated, the modelling using wished-in-place struts underestimates the strut force in the initial stages. Most importantly, the effect of daily and yearly temperature variations on the monitored strut forces is significant, which the current model is unable to capture as temperature effects are not considered. There is a general decrease in strut forces from September to November 2003 (autumn), followed by a major increase from March to September 2004 (spring & summer), this is corroborated

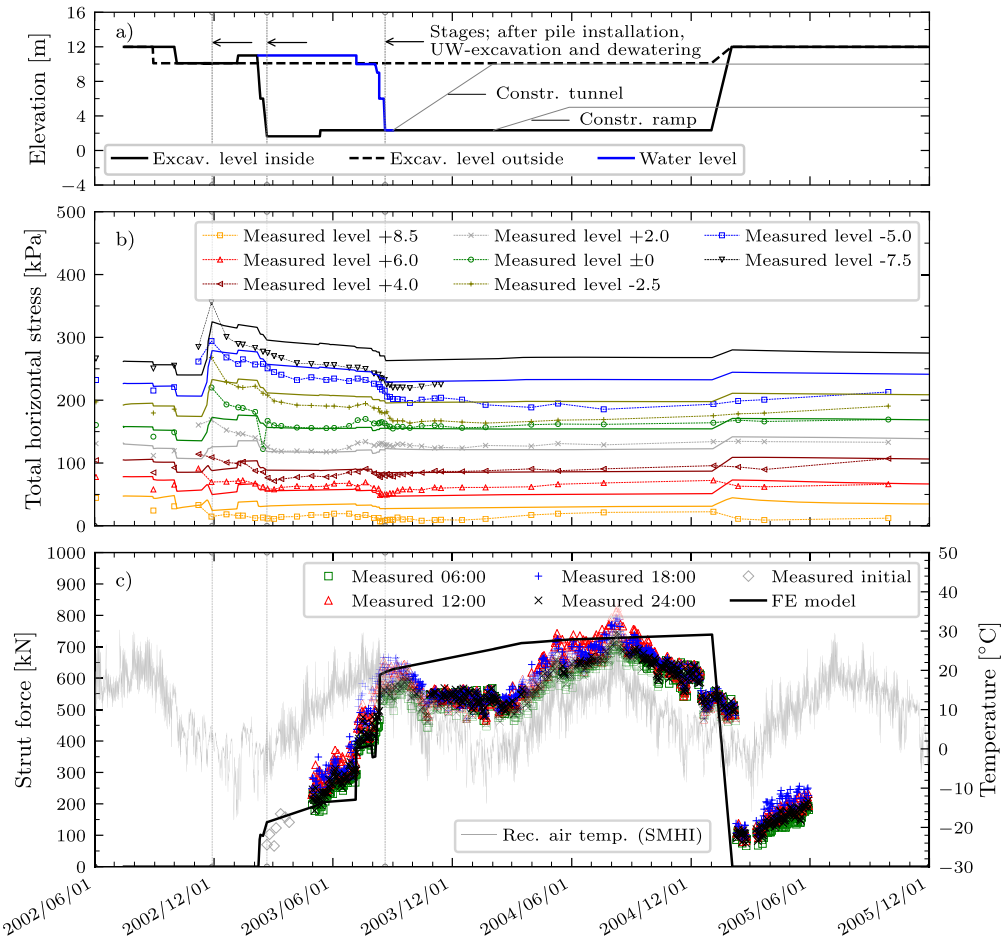

Fig. 16. Measured and computed horizontal total stresses and the strut force a) construction sequence, b) total stresses at 0.5 m distance behind SPW and c) strut force. Solid lines with no symbols indicate computed results.

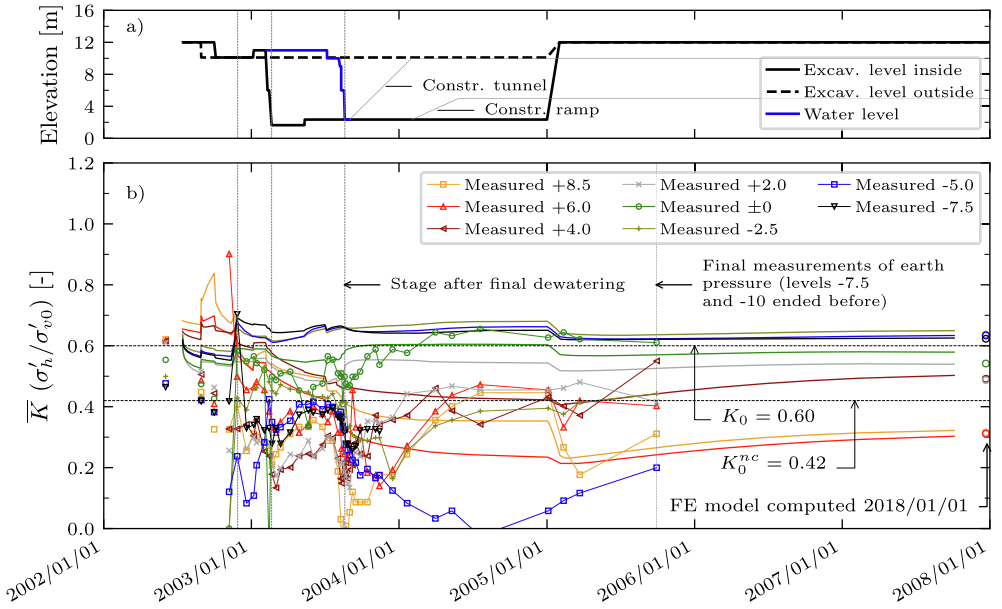

Fig. 17. a) construction sequence and b) measured and computed normalised horizontal stress denoted $\overline{K}=\sigma_h'/\sigma_{v0}'$ at location of earth pressure cells (0.5 m behind SPW). Solid lines with no symbols indicate computed results.

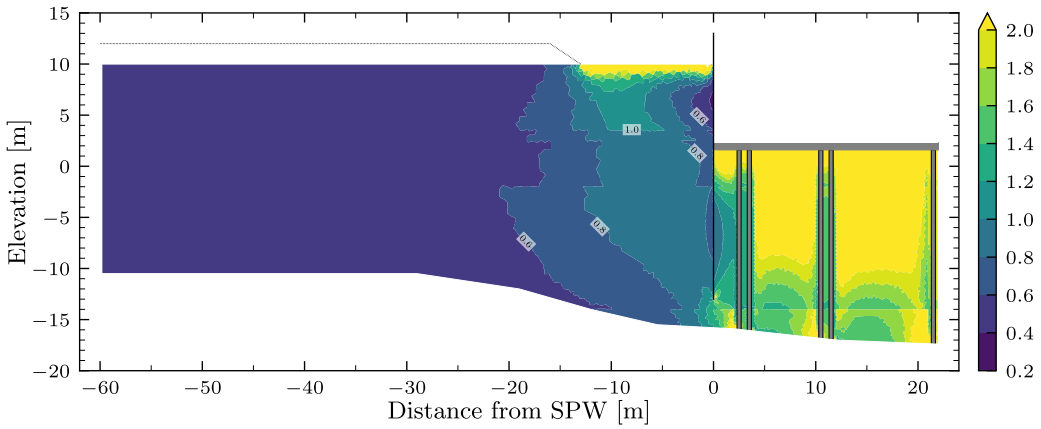

Fig. 18. Computed results for $K=\sigma_h'/\sigma_v'$ in clay layers at the stage after final dewatering.

Table 4
Measured and computed background settlement rates.

	Prior construction	Present day max
Measured	3–8 mm/yr (Svahn and Liedberg, 2001)	2–6 mm/yr (InSAR)
Computed	6.2 mm/yr	3.5 mm/yr

by the trend in the recorded air temperature. The effects of temperature have been also been highlighted by Whittle et al. (1993).

Fig. 17 presents the normalised horizontal earth pressures, denoted as a proxy to earth pressure coefficient, as the vertical total stress was not measured. The normalised horizontal earth pressure is calculated as $\overline{K}=\sigma_h'/\sigma_{v0}'$, where σ_h' is the horizontal effective stress and σ_{v0}' the in situ vertical effective stress at the start of construction. The measured values of σ_h' are obtained from $\sigma_{h,TPcells}$ - $u_{TPcells}$, while the computed values are obtained directly from the numerical model. To understand the spatial variation of the earth pressure coefficient $K=\sigma_h'/\sigma_v'$, the simulation

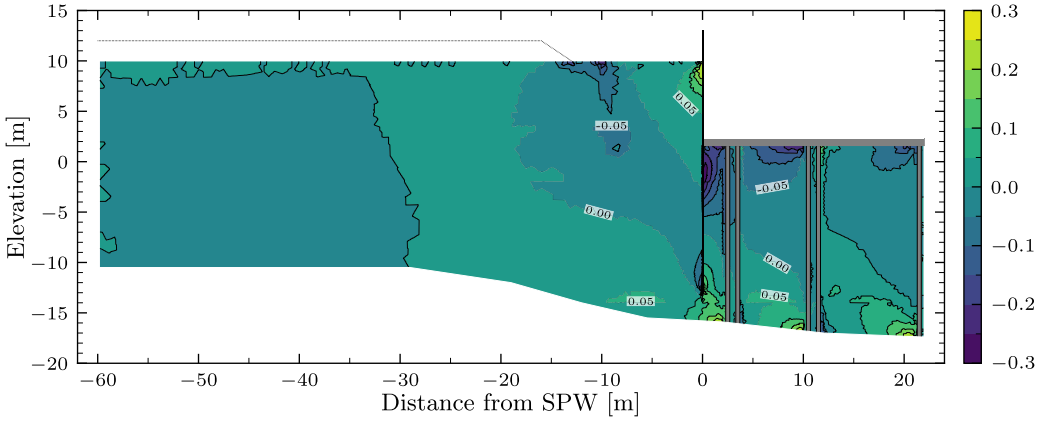

Fig. 19. Evolving anisotropy α_{xy} after final dewatering.

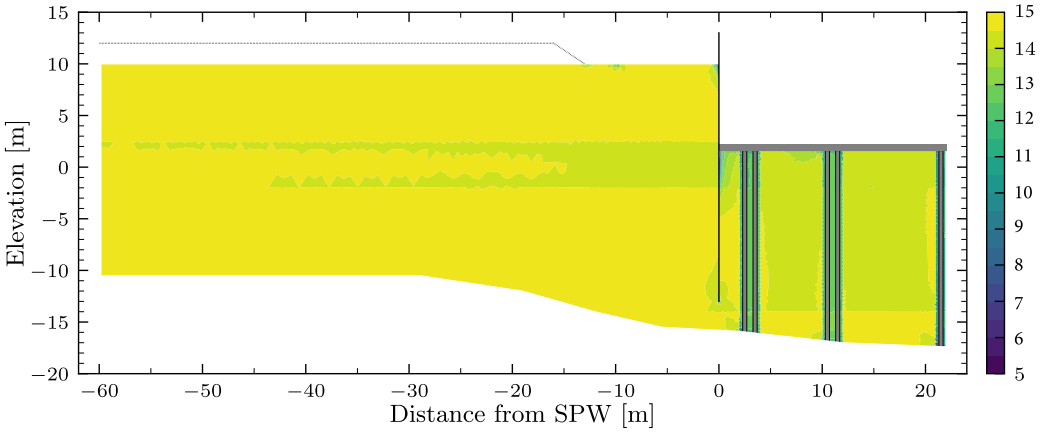

Fig. 20. Destructuration χ after final dewatering.

results at the stage after the final dewatering are presented in Fig. 18. This illustrates the effect of wall displacements, as K approaches the lower values between the support levels of the struts and the slab.

The results in Figs. 17 and 18 highlight the variation of horizontal stresses both with location and time. The apparent scatter in the measurement data in Fig. 17 comes from the impact of construction activities including installation effects, resulting in time-dependent induced stresses and the rotation of principal stresses. In addition, the relative stiffness of the soil and the structure vary with depth (due to e.g. the support levels of struts and concrete slab), as seen in Fig. 18. The relative stiffness will also affect the long-term K.

4.3. Background creep settlement rates

The computed long-term settlement rates are listed in Table 4, including the measured settlement rates, as described in Section 2.1. When using a rate-dependent model, the settlement rates prior to construction need to be checked against available monitoring data, before proceeding with the remainder of the modelling. Overall, the construction of the tunnel has reduced the background settlement rates compared to the situation before the construction. The current ongoing background settlement rate was computed to be a maximum of 3.5 mm/year in the studied cross section, which compares well to the measurement data (InSAR data presented in Fig. 3).

4.4. Role of evolving anisotropy and destructuration

Some additional results of the construction phase are presented to investigate the impact of evolving anisotropy and destructuration in modelling of the Göta Tunnel excavation. In Fig. 19 the rotation of the Normal Compression Surface is illustrated by a plot of α_{xy}, the "distortional" component of the fabric tensor, after the final dewatering. The initial value of α_{xy} was equal to zero. The results demonstrate that there is significant evolution of anisotropy which is not surprising, given the problem of deep excavation involves also significant stress rotations (Whittle et al., 1993). Thus, the evolution of anisotropy cannot be ignored. The fact that significant changes in α_{xy} are computed up to 30 m from the SPW indicates that the elasto-viscoplastic zone is rather large.

Similarly, in Fig. 20 the role of destructuration is studied by plotting the value of the state parameter that describes the amount of bonding, χ, which had initial value $\chi_0 = 15$. Clearly, no major destructuration is computed in the majority of the domain, except in the vicinity of the piles. The slightly darker area between level +2.5 and −2.0 are due to the low OCR value (=1.1) in this the clay layer. The main benefit of including bonding and destructuration is thus the ability to use the concept in modelling the installation effects of the pre-fabricated displacement piles. Given there is no significant evolution of the structure parameter elsewhere in the domain, the conventional design of excavations can exploit the peak undrained shear strength, provided the deformations are kept at a reasonable low level. The results, furthermore, indicate that the changes in anisotropy due to rotation of principal stresses is more important than the stiffness degradation.

5. Conclusions

An advanced rate-dependent constitutive model for soft soils, CreepSCLAY1S, has been successfully benchmarked at boundary value level on a deep excavation in soft sensitive clay. An instrumented section of Göta Tunnel provided the necessary monitoring data on horizontal and vertical displacements, pore pressures and horizontal stress at several locations, covering the complete construction period of approximately 3 years.

A consistent set of model parameters was evaluated and calibrated using the common laboratory tests available, including CRS oedometer tests and K_0-consolidated undrained triaxial tests sheared in compression and extension. IL oedometer tests from a nearby project were used to estimate the intrinsic creep rate. As the model is rate-dependent, the strain-rates used in the laboratory are automatically related to the strain rates in the field.

Several modelling phases were needed to create an appropriate initial state for the numerical model, which was found to match the background settlement rates before construction. Subsequently, the project log-books were used to reproduce the actual timeline of the construction stages. The features relating to bonding and destructuration in the constitutive model were exploited to account for the most important installation effects, such as the installation of piles at the bottom of the excavation, which for simplicity were modelled with prescribed volumetric strains.

The trends in the horizontal and vertical displacements as a function of time were reproduced satisfactorily by the numerical simulations. The match between the computed results and measurements, however, reduced with increasing distance from the sheet pile wall. As it was not possible to model all construction operations, not all features of the excavation response were reproduced. For example, the persistent ongoing horizontal movements and vertical settlements behind the sheet pile wall after dewatering were not properly captured.

The evolution of the pore pressures, as a function of depth and distance to the wall, were captured with high fidelity by the model, as well as the horizontal total stresses and the strut forces. Most importantly, the results demonstrate that the rate-dependent model used allows to model the complete service life of the tunnel, from construction of the excavation to the tunnel operation, with one unified model parameter set. Not only were the background settlements rates reproduced, but also the current on-going settlements next to Göta Tunnel, measured with InSAR satellite data.

Overall, the results are very encouraging, even though the constitutive model does not account for the degradation of the small-strain stiffness. Perhaps such a feature is not as important when dealing with soft sensitive clays. The small strain stiffness may, however, be one of the reasons why the computed deformations deviate more from the measurements further away from the excavation. Future research will quantify the importance of small-strain stiffness for the design of underground structures in soft clay.

The computed earth pressures indicate that optimisation aided by FE analyses would be preferable as opposed to design based on limit equilibrium analyses. Combined with a rate-dependent constitutive model, FE analyses provide tools to assess the effects of the construction process and the relative soil-wall stiffness on the long-term earth pressures. Additionally, this enables taking into account geometry effects, as well as the construction activities outside the perimeter of the retaining wall, including the potential increase of earth pressures due to creep deformations.

In conclusion, excavations in urban areas are complex problems, given the proximity to existing buildings and infrastructure, as well as the level of detail needed in modelling the anthropogenic loading history, construction sequence, soil-structure interaction and even temperature effects. In sensitive clays, the installation effects, in particular the disturbance of the soil due to the installation of piles and anchors are important to account for.

As it may be challenging to estimate the construction time-steps beforehand, it would be advisable to update the model as the construction proceeds as part of the implementation of the Observational Method. Capturing time-dependent process is not only important during construction time, but also in the long-term. As demonstrated by this paper and e.g. Whittle et al. (2015) and Rouainia et al. (2017), accurate prediction can be made with a well-calibrated constitutive model that has the features necessary for the geotechnical problem in consideration.

CRediT authorship contribution statement

Johannes Tornborg: Conceptualization, Methodology, Formal

analysis, Writing - original draft, Visualization. **Mats Karlsson:** Supervision. **Anders Kullingsjö:** Investigation, Data curation. **Minna Karstunen:** Writing - review & editing.

Declaration of Competing Interest

The authors declare that they have no known competing financial interests or personal relationships that could have appeared to influence the work reported in this paper.

Acknowledgements

The financial support provided by Skanska, SBUF (Development fund of the Swedish construction industry, grant 13416), BIG (Better Interaction in Geotechnics, grant A2018-09, from the Swedish Transport Administration) and Formas (grant 2016-01428) are greatly acknowledged. The work is done as part of Digital Twin Cities Centre that is supported by Sweden's Innovation Agency VINNOVA. Finally, the authors would like to thank Jelke Dijkstra and Ayman Abed for their valuable comments.

Appendix A. Brief description of the Creep-SCLAY1S model

The Creep-SCLAY1S model is essentially a rate-dependent extension of the Modified Cam Clay (MCC) model. Additionally, the model also incorporates anisotropy and destructuration at large strains. For a complete generalised description of the model see Sivasithamparam et al. (2015).

The total strain is composed of elastic and viscoplastic (creep) strains according to:

$$\dot{\varepsilon} = \dot{\varepsilon}^{e} + \dot{\varepsilon}^{c} \tag{A.1}$$

The dot symbol refers to strain rate (differentiation w.r.t. time). Note that there is no purely elastic region. Isotropic non-linear elasticity is assumed according to the MCC model.

The model incorporates a normal compression surface (NCS) which in triaxial stress space is defined by a sheared ellipse according to:

$$f_{NCS} = (q - \alpha p')^2 - \left(M(\theta)^2 - \alpha^2\right)\left(p'_m - p'\right)p' = 0 \tag{A.2}$$

where $M(\theta)$ is the Lode angle dependent value of M, the stress ratio at critical state.

The current and intrinsic stress states are described by two additional surfaces; the current stress surface (CSS) and the intrinsic compression surface (ICS) according to Fig. A1.

The size of the intrinsic and normal compression surfaces are related to the state variable χ, describing the current amount of structure in the soil:

$$p'_m = (1+\chi)p'_{mi} \tag{A.3}$$

The model incorporates three hardening laws relating to the volumetric hardening, the evolution of anisotropy and destructuration, respectively. The volumetric hardening is controlled by:

$$dp'_{mi} = \frac{p'_{mi}}{\lambda^*_i - \kappa^*} d\varepsilon^c_v \tag{A.4}$$

The evolution of anisotropy is controlled by:

$$d\alpha = \omega\left[\left(\frac{3\eta}{4} - \alpha\right)\left\langle d\varepsilon^c_v \right\rangle + \omega_d\left(\frac{\eta}{3} - \alpha\right)\left|d\varepsilon^c_q\right|\right] \tag{A.5}$$

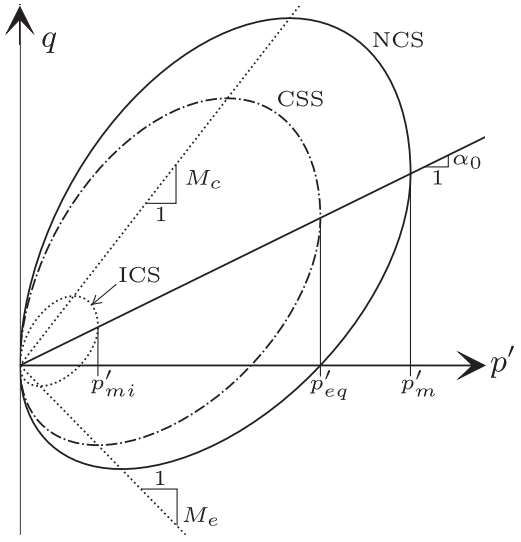

Fig. A1. Illustration of intrinsic, current stress and normal compression surfaces of the Creep-SCLAY1S model.

The degradation of bonding (destructuration) is controlled by:

$$d\chi = -a\chi\left[\left|d\varepsilon_v^c\right| + b\left|d\varepsilon_q^c\right|\right] \tag{A.6}$$

The viscoplastic strain rates are calculated (assuming an associated flow rule) according to:

$$\dot{\varepsilon}_v^c = \dot{\Lambda}\frac{\partial p_{eq}^{'}}{\partial p^{'}} \text{and} \dot{\varepsilon}_q^c = \dot{\Lambda}\frac{\partial p_{eq}^{'}}{\partial q} \tag{A.7}$$

where $\dot{\Lambda}$ is the (rate-dependent) viscoplastic multiplier defined as:

$$\dot{\Lambda} = \underbrace{\frac{\mu_i^*}{\tau_{ref}}\left(\frac{p_{eq}^{'}}{p_m^{'}}\right)^{\frac{\lambda_i^*-\kappa^*}{\mu_i^*}}}_{\text{i)}}\underbrace{\left(\frac{M^2\left(\theta\right)-\alpha_{K_0^{nc}}^2}{M^2\left(\theta\right)-\eta_{K_0^{nc}}^2}\right)}_{\text{ii)}} \tag{A.8}$$

where the ii) term is added to ensure that the predicted creep strain rate reduce to i) for the oedometric conditions.

Appendix B. Parameter sets for structural elements and calculations phases in modelling of Göta Tunnel

Table B1
Parameter sets for structural elements.

Structural element	Material set	Parameter	Value
UW-concrete slab	Mohr-Coloumb	ρ	2.4 t/m^3
	(Drained)	E	30 GPa
		ν	0.20 [–]
		$c^{'}$	2.0 MPa
		$\phi^{'}$	35°
		$k_h = k_v$	1×10^{-9} m/s [a]
		K_0	1.0 [–]
		R_{inter}	0.2 [–]
		Tension-cut off	Yes (1.6 MPa)
UW-concrete slab for SPW interface [b]	Mohr-Coloumb (Non-porous)	ρ, E, ν, K_0, and R_{inter}	As above
		$c^{'}$	200 kPa
		$\phi^{'}$	0°
		Tension-cut off	Yes (0 MPa)
Struts ∅711–14.2 mm	Fixed-end-anchor	E	210 GPa
		A	311 cm^2
		c.t.c-distance	9.0 m
Sheet pile walls (AZ36)	Plate	E	210 GPa
		EA	5.2×10^6 kN/m
		EI	174×10^3 kN/m^2/m
		w	1.9 kN/m/m
		ν	0.30 [–]
		M_p	1448 kNm/m
		N_p	8552 kN/m
Concrete piles (0.4×0.4 m^2)	Emb. beam rows	E	37 GPa
		c.t.c-distance	2.4 m [c]
		$T_{axial,skin}$	$f(0.7c_u)$ kN/m
		$T_{lat,skin}$	1 kN/m

[a] Due to the number of concrete piles and vertical anchors perforating the slab, it was assigned a permeability ($k = 1\times10^{-9}$ m/s) equal to that of the clay.
[b] For the concrete interface connected to the SPW, a separate material set was created with the tension cut-off set to 0 kPa in order to allow for the concrete to separate from the SPW in tension.
[c] 2.0 m in the pile row in the tunnel centerline.

Table B2
Calculation phases in the FE-analysis.

Phase	Description	Time [days]
01	Initial stress generation (gravity loading)	-
02	Change to model Poisson's ratio (0.20)	-
03	NIL-step	-
04[a]	Installation of SPW	1 (44)
05	Excavation to level +10 (eastern part)	1 (32)
06	Excavation to level +10 (within SPW)	4 (38)
07	Pile install. at Section 1/430 of centreline rows	8 (-)
08	Pile install. at Section 1/430 middle rows in middle	2 (-)
09	Pile install. at Section 1/430 of rows closest to SPW	6 (-)
10	Activate embedded beams	1 (37)
11	Fill to +11 within SPW	2 (29)
12	Underwater excav. to level +9	2 (-)
13	Underwater excav. to level +7 and strut installation	2 (-)
14	Underwater excav. to level +6	1 (4)
15	Underwater excavation to final level (+1.6)	6 (79)
16	Casting of 0.7 m thick concrete slab	2 (14)
17	Installation and pre-stressing of vertical anchors	37 (4)
18	Dewatering to level +10	1 (23)
19	Extended unloading excav. (level +10) outside SPW	2 (4)
20	Dewatering to level +9	3 (3)
21	Dewatering to level +6	1 (7)
22	Final dewatering	2 (12)
23	Construction of main tunnel	153 (-)
24	Fill on slab for construction of ramp segment	42 (17)
25	Construction of ramp segment	57 (218)
26	Back-filling to level +12 and cut strut	31 (15)
27	Consolidation 2005 to 2018	5081 (-)
28	Consolidation for 2019 settlement rate	365 (-)

All phases except 01–03 are calculated as consolidation analysis. Execution times and stall/consolidation times, given within (), after respective activity are based on the project logbooks.

[a] Start 2002–07-15.

References

Amavasai, A., Gras, J.P., Sivasithamparam, N., Karstunen, M., Dijkstra, J., 2017. Towards consistent numerical analyses of embankments on soft soils. Eur. J. Environ. Civil Eng. 8189, 1–19. https://doi.org/10.1080/19648189.2017.1354784.

Amavasai, A., Sivasithamparam, N., Dijkstra, J., Karstunen, M., 2018. Consistent Class A & C predictions of the Ballina test embankment. Comput. Geotech. 93 (2018), 75–86. https://doi.org/10.1016/j.compgeo.2017.05.025.

Bertoldo, F., Callisto, L., 2016. Effect of consolidation on the behaviour of excavations in fine-grained soils. Procedia Eng. 158, 344–349. https://doi.org/10.1016/j.proeng.2016.08.453.

Bertoldo, F., Callisto, L., 2019. Delayed response of excavations in structured clays. Can. Geotech. J. 56 (11), 1584–1595. https://doi.org/10.1139/cgj-2018-0512.

Bjerrum, L., 1967. Engineering geology of norwegian normally-consolidated marine clays as related to settlements of buildings. Géotechnique 17 (2), 83–118. https://doi.org/10.1680/geot.1967.17.2.83.

Callisto, L., Calabresi, G., 1998. Mechanical behaviour of a natural soft clay. Géotechnique 48 (4), 495–513. https://doi.org/10.1680/geot.1998.48.4.495.

Carder, D.R., Darley, P., 1998. The long term performance of embedded retaining walls. Tech. rep., Transport Research Laboratory, Crowthorne.

Castro, J., Karstunen, M., Sivasithamparam, N., 2014. Influence of stone column installation on settlement reduction. Comput. Geotech. 59, 87–97. https://doi.org/10.1016/j.compgeo.2014.03.003.

Chen, R.P., Li, Z.C., Chen, Y.M., Ou, C.Y., Hu, Q., Rao, M., 2015. Failure investigation at a collapsed deep excavation in very sensitive organic soft clay. J. Performance Construct. Facilities 29 (3). https://doi.org/10.1061/(ASCE)CF.1943-5509.0000557, 04014078-1.

Chowdhury, S.S., Deb, K., Sengupta, A., 2013. Estimation of design parameters for braced excavation: numerical study. Int. J. Geomech. 13 (3), 234–247. https://doi.org/10.1061/(ASCE)GM.1943-5622.0000207.

Corral, G., Whittle, A.J., 2010. Re-analysis of deep excavation collapse using a generalized effective stress soil model. In: Earth Retention Conference. American Society of Civil Engineers, Bellevue, pp. 720–731. https://doi.org/10.1061/41128(384)72.

Crawford, C.B., 1964. Interpretation of the consolidation test. J. Soil Mech. Found. Division 90 (5), 87–102.

Do, T.-N., Ou, C.-Y., Chen, R.-P., 2016. A study of failure mechanisms of deep excavations in soft clay using the finite element method. Comput. Geotech. 73 (2016), 153–163. https://doi.org/10.1016/j.compgeo.2015.12.009.

Dong, Y.P., Burd, H.J., Houlsby, G.T., 2016. Finite-element analysis of a deep excavation case history. Géotechnique 66 (1), 1–15. https://doi.org/10.1680/jgeot.14.P.234.

Fang, H.-Y. (Ed.), 1991. Foundation Engineering Handbook, 2nd ed. Springer, US, Boston. https://doi.org/10.1007/978-1-4615-3928-5.

Finno, R.J., Nerby, S.M., 1989. Saturated clay response during braced cut construction. J. Geotech. Eng. 115 (8), 1065–1084. https://doi.org/10.1061/(ASCE)0733-9410(1989)115:8(1065).

Finno, R.J., Roboski, J.F., 2005. Three-dimensional responses of a tied-back excavation through clay. J. Geotech. Geoenviron. Eng. 131 (3), 273–282. https://doi.org/10.1061/(ASCE)1090-0241(2005)131:3(273).

Finno, R.J., Blackburn, J.T., Roboski, J.F., 2007. Three-dimensional effects for supported excavations in clay. J. Geotech. Geoenviron. Eng. 133 (1), 30–36. https://doi.org/10.1061/(ASCE)1090-0241(2007)133:1(30).

Graham, J., Crooks, J.H., Bell, A.L., 1983. Time effects on the stress-strain behaviour of natural soft clays. Geotechnique 33 (3), 327–340. https://doi.org/10.1680/geot.1983.33.3.327.

Gras, J.P., Sivasithamparam, N., Karstunen, M., Dijkstra, J., 2017. Strategy for consistent model parameter calibration for soft soils using multi-objective optimisation. Comput. Geotech. 90, 164–175. https://doi.org/10.1016/j.compgeo.2017.06.006.

Gras, J.P., Sivasithamparam, N., Karstunen, M., Dijkstra, J., 2018. Permissible range of model parameters for natural fine-grained materials. Acta Geotech. 13 (2), 387–398. https://doi.org/10.1007/s11440-017-0553-1.

Hashash, Y.M.A., Whittle, A.J., 1996. Ground movement prediction for deep excavations in soft clay. J. Geotech. Eng. 122 (6), 474–486. https://doi.org/10.1061/(ASCE)0733-9410(1996)122:6(474).

Jardine, R.J., Potts, D.M., Fourie, A.B., Burland, J.B., 1986. Studies of the influence of non-linear stress–strain characteristics in soil–structure interaction. Géotechnique 36 (3), 377–396. https://doi.org/10.1680/geot.1986.36.3.377.

Karlsrud, K., Andresen, L., 2008. Design and performance of deep excavations in soft clays. In: 6th International Conference on Case Histories in Geotechnical Engineering, Arlington, pp. 1–26.

Karlsrud, K., Hernandez-Martinez, F.G., 2013. Strength and deformation properties of Norwegian clays from laboratory tests on high-quality block samples. Can. Geotech. J. 50 (12), 1273–1293. https://doi.org/10.1139/cgj-2013-0298.

Karlsson, M., Yannie, J., Dijkstra, J., 2019. Modeling aging of displacement piles in natural soft clay. J. Geotech. Geoenviron. Eng. 145 (10) https://doi.org/10.1061/(ASCE)GT.1943-5606.0002110, 04019070–1.

Karstunen, M., Koskinen, M., 2008. Plastic anisotropy of soft reconstituted clays. Can. Geotech. J. 45 (3), 314–328. https://doi.org/10.1139/T07-073.

Karstunen, M., Krenn, H., Wheeler, S.J., Koskinen, M., Zentar, R., 2005. Effect of anisotropy and destructuration on the behavior of murro test embankment. Int. J. Geomech. 5 (2), 87–97. https://doi.org/10.1061/(ASCE)1532-3641(2005)5:2(87).

Kempfert, B., Gebresellassie, H.G., 1999. Effect of anchor installation on settlement of nearby structures in soft soils. In: International symposium on Geotechnical Aspects of Underground Construction in Soft Ground, Tokyo, pp. 665–670.

Kullingsjö, A., 2007. Effects of deep excavations in soft clay on the immediate surroundings. Doctoral dissertation. Chalmers University of Technology, Gothenburg.

Lande, E., Karlsrud, K., 2015. Feltforsøk stagboring - Dokumentasjon av effekter ved boring i leire. Tech. rep., NGI, Oslo.
Larsson, R., 1981. Drained behaviour of Swedish clays. Tech. rep., Swedish Geotechnical Institute, Linköping.
Larsson, P.-G., 2018. Geotechnical site investigation report. Tech. rep., Bohusgeo AB, Uddevalla.
Lefebvre, G., LeBoeuf, D., 1987. Rate effects and cyclic loading of sensitive clays. J. Geotechn. Eng. 113 (5), 476–489. https://doi.org/10.1061/(ASCE)0733-9410(1987)113:5(476).
Leroueil, S., Vaughan, P.R., 1990. The general and congruent effects of structure in natural soils and weak rocks. Geotechnique 40 (3), 467–488. https://doi.org/10.1680/geot.1990.40.3.467.
Magnus, R., Teh, C.I., Lau, J.M., 2005. Report on the incident at the MRT Circle Line worksite that led to the collapse of the Nicoll Highway on 20 April 2004, Tech. rep., Ministry of Manpower, Singapore.
Olsson, M., 2013. On rate-dependency of Gothenburg clay. Doctoral dissertation. Chalmers University of Technology, Gothenburg. https://doi.org/10.13140/RG.2.1.2241.3843.
Orazalin, Z.Y., Whittle, A.J., Olsen, M.B., 2015. Three-dimensional analyses of excavation support system for the stata center basement on the MIT campus. J. Geotech. Geoenviron. Eng. 141 (7), 05015001. https://doi.org/10.1061/(ASCE)GT.1943-5606.0001326.
Pande, G.N., Sharma, K.G., 1983. Multi-laminate model of clays - a numerical evaluation of the influence of rotation of the principal stress axes. Int. J. Numer. Anal. Meth. Geomech. 7 (4), 397–418. https://doi.org/10.1002/nag.1610070404.
Peck, R.B., 1969. Advantages and limitations of the observational method in applied soil mechanics. Géotechnique 19 (2), 171–187. https://doi.org/10.1680/geot.1969.19.2.171.
Potts, D.M., Fourie, A.B., 1984. The behaviour of a propped retaining wall: Results of a numerical experiment. Geotechnique 34 (3), 383–404. https://doi.org/10.1680/geot.1984.34.3.383.
Richards, D.J., Powrie, W., Roscoe, H., Clark, J., 2007. Pore water pressure and horizontal stress changes measured during construction of a contiguous bored pile multi-propped retaining wall in Lower Cretaceous clays. Géotechnique 57 (2), 197–205. https://doi.org/10.1680/geot.2007.57.2.197.
Rouainia, M., Elia, G., Panayides, S., Scott, P., 2017. Nonlinear finite-element prediction of the performance of a deep excavation in boston blue clay. J. Geotech. Geoenviron. Eng. 143 (5), 04017005. https://doi.org/10.1061/(ASCE)GT.1943-5606.0001650.
Sällfors, G., 1975. Preconsolidation pressure of soft, high-plastic clays. Doctoral dissertation. Chalmers University of Technology, Gothenburg.
Scharinger, F., Schweiger, H.F., Pande, G.N., 2009. On a multilaminate model for soil incorporating small strain stiffness. Int. J. Numer. Anal. Meth. Geomech. 33 (2), 215–243. https://doi.org/10.1002/nag.710.
Schmidt, B., 1966. Earth pressures at rest related to stress history. Can. Geotech. J. 3 (4), 239–242. https://doi.org/10.1139/t66-028.
Shen, S.L., Wu, H.N., Cui, Y.J., Yin, Z.Y., 2014. Long-term settlement behaviour of metro tunnels in the soft deposits of Shanghai. Tunn. Undergr. Space Technol. 40, 309–323. https://doi.org/10.1016/j.tust.2013.10.013.
Sivasithamparam, N., Karstunen, M., Bonnier, P., 2015. Modelling creep behaviour of anisotropic soft soils. Comput. Geotech. 69 (2015), 46–57. https://doi.org/10.1016/j.compgeo.2015.04.015.
Svahn, P.-O., Liedberg, S., 2001. Väg 45 Götatunneln - Järntorget, entreprenad J2, PM Tråg/tunnel 1/160-1/350. Tech. rep., Skanska Sverige AB, Göteborg.
Swedish Meteorological and Hydrological Institute, 2020. Air temperature recordings. Station Gothenburg A. https://www.smhi.se/data/meteorologi/.
Tornborg, J., Karlsson, M., Karstunen, M., 2019. Benchmarking of a contemporary soil model for simulation of deep excavations in soft clay. In: 17th European Conference on Soil Mechanics and Geotechnical Engineering, pp. 721–728.
Wheeler, S.J., Näätänen, A., Karstunen, M., Lojander, M., 2003. An anisotropic elastoplastic model for soft clays. Can. Geotech. J. 40 (2), 403–418. https://doi.org/10.1139/t02-119.
Whittle, A.J., Hashash, Y.M.A., Whitman, R.V., 1993. Analysis of deep excavation in boston. J. Geotech. Eng. 119 (1), 69–90. https://doi.org/10.1061/(ASCE)0733-9410(1993)119:1(69).
Whittle, A.J., Corral, G., Jen, L.C., Rawnsley, R.P., 2015. Prediction and performance of deep excavations for courthouse station, Boston. J. Geotech. Geoenviron. Eng. 141 (4) https://doi.org/10.1061/(asce)gt.1943-5606.0001246, 04014123-1.
Wu, H.-N., Shen, S.-L., Yang, J., 2017. Identification of tunnel settlement caused by land subsidence in soft deposit of Shanghai. J. Performance Constructed Facilit. 31 (6), 04017092. https://doi.org/10.1061/(ASCE)CF.1943-5509.0001082.
Zdravkovic, L., Potts, D.M., St, H.D., 2005. John, Modelling of a 3D excavation in finite element analysis. Geotechnique 55 (7), 497–513. https://doi.org/10.1680/geot.2005.55.7.497.
Zeevaert, L., 1957. Foundation design and behaviour of tower Latino Americana in Mexico City. Géotechnique 7 (3), 115–133. https://doi.org/10.1680/geot.1957.7.3.115.